Research paper

Heterozygosity for *Nuclear Factor One X* in mice models features of Malan syndrome

Sabrina Oishi [a], Danyon Harkins [a], Nyoman D. Kurniawan [b], Maria Kasherman [a,c], Lachlan Harris [a,d], Oressia Zalucki [a], Richard M. Gronostajski [e], Thomas H.J. Burne [f,g], Michael Piper [a,f,*]

[a] The School of Biomedical Sciences, The University of Queensland, Brisbane, QLD 4072, Australia
[b] The Centre for Advanced Imaging, The University of Queensland, Brisbane, QLD 4072, Australia
[c] Griffith Institute for Drug Discovery, Griffith University, Brisbane, QLD 4111, Australia
[d] The Francis Crick Institute, 1 Midland Road, King's Cross, London, United Kingdom
[e] Department of Biochemistry, Program in Genetics, Genomics and Bioinformatics, Center of Excellence in Bioinformatics and Life Sciences, State University of New York at Buffalo, Buffalo, NY 14203, USA
[f] The Queensland Brain Institute, The University of Queensland, Brisbane, QLD 4072, Australia
[g] Queensland Centre for Mental Health Research, The Park Centre for Mental Health, Wacol, Brisbane, QLD 4076, Australia

ARTICLE INFO

ABSTRACT

Background: Nuclear Factor One X (*NFIX*) haploinsufficiency in humans results in Malan syndrome, a disorder characterized by overgrowth, macrocephaly and intellectual disability. Although clinical assessments have determined the underlying symptomology of Malan syndrome, the fundamental mechanisms contributing to the enlarged head circumference and intellectual disability in these patients remains undefined.
Methods: Here, we used *Nfix* heterozygous mice as a model to investigate these aspects of Malan syndrome. Volumetric magnetic resonance imaging (MRI) was used to calculate the volumes of 20 brain sub regions. Diffusion tensor MRI was used to perform tractography-based analyses of the corpus callosum, hippocampal commissure, and anterior commissure, as well as structural connectome mapping of the whole brain. Immunohistochemistry examined the neocortical cellular populations. Two behavioral assays were performed, including the active place avoidance task to assess spatial navigation and learning and memory function, and the 3-chambered sociability task to examine social behaviour.
Findings: Adult $Nfix^{+/-}$ mice exhibit significantly increased brain volume (megalencephaly) compared to wildtypes, with the cerebral cortex showing the highest increase. Moreover, all three forebrain commissures, in particular the anterior commissure, revealed significantly reduced fractional anisotropy, axial and radial diffusivity, and tract density intensity. Structural connectome analyses revealed aberrant connectivity between many crucial brain regions. Finally, $Nfix^{+/-}$ mice exhibit behavioral deficits that model intellectual disability.
Interpretation: Collectively, these data provide a significant conceptual advance in our understanding of Malan syndrome by suggesting that megalencephaly underlies the enlarged head size of these patients, and that disrupted cortical connectivity may contribute to the intellectual disability these patients exhibit.
Fund: Australian Research Council (ARC) Discovery Project Grants, ARC Fellowship, NYSTEM and Australian Postgraduate Fellowships.

1. Introduction

Malan syndrome (MIM #614753) is caused by mutations in the *Nuclear Factor One-X* (*NFIX*) gene in humans [1]. Heterozygous *NFIX* deletions or nonsense/missense mutations in the DNA-binding/dimerization domain (exon 2/3) of *NFIX* (MIM #164005), located at chromosome 19p13.2, results in loss of protein function, which is referred to as *NFIX* haploinsufficiency [1–4]. The clinical features of Malan syndrome include prenatal and childhood overgrowth, developmental delays, macrocephaly (head circumference >2 standard deviation from the corresponding age of the population), intellectual disability, and autistic-like traits [1,5]. Patients also exhibit advanced bone age and stereotypical craniofacial features [1,5]. Recently, a review of Malan syndrome patients summarized that while the majority (60 out of 79 cases) of patients had macrocephaly, neuroimaging showed relatively normal brain structure in most patients with the occasional

* Corresponding author at: The School of Biomedical Sciences, The University of Queensland, Brisbane, QLD 4072, Australia.
 E-mail address: m.piper@uq.edu.au (M. Piper).

Research in context

Evidence before this study

Nuclear Factor One X (*NFIX*) haploinsufficiency in humans results in Malan syndrome, a disorder characterized by overgrowth, macrocephaly and intellectual disability. Although clinical assessments have determined the underlying symptomology of Malan syndrome, the fundamental mechanisms contributing to their enlarged head circumference and intellectual disability in these patients remains undefined.

Added value of the study

This study used *Nfix* heterozygous mice as a model to investigate these aspects of Malan syndrome. Using magnetic resonance imaging, this study reveals that brain volume (termed as megalencephaly) is significantly increased within adult *Nfix*$^{+/-}$ mice, most markedly within the cerebral cortex. Moreover, using diffusion magnetic resonance imaging and tractography-based analyses, we reveal microstructural deficits within major forebrain commissures and aberrant connectivity between many crucial brain regions. Finally, we demonstrate that *Nfix*$^{+/-}$ mice exhibit cortically-mediated behavioral deficits that model intellectual disability.

Implications of all the available evidence

Collectively, these data suggest that the macrocephaly exhibited within Malan syndrome likely arises from megalencephaly, as well as providing insights into the structural and behavioral correlates underlying the intellectual disability of these patients. In summary, this study models brain structure and behavior in *Nfix* heterozygous mice to provide a significant conceptual advance in our understanding of the factors underlying Malan syndrome. These findings suggest that future assessments of Malan syndrome patients could include high-resolution neuroimaging, such as DTMRI and tractography, to identify megalencephaly and aberrant brain connectivity.

non-specific abnormality such as enlarged ventricles, small callosal bodies, and cortical dysplasia [5]. Macrocephaly is clinically distinct from megalencephaly, as the latter refers to enlargements of brain size and weight [6–8]. Notably, megalencephaly can underlie macrocephaly and both can be associated within the same developmental disorder [6,7]. Therefore, it is possible that the macrocephaly phenotype featured in Malan syndrome patients is due to megalencephaly. However, other than basic clinical assessment of these patients, the cause of macrocephaly in these patients remains unclear, as is whether these patients exhibit normal connectivity within the brain.

Here, we used mice lacking one allele of *Nfix* as a model to probe these aspects of Malan syndrome. NFIX in rodents is crucial for the development of numerous regions of the central nervous system, including the neocortex [9], hippocampus [10,11], and cerebellum [12], as well as in skeletal muscle formation [13,14]. At a mechanistic level, NFIX promotes the asymmetric division of neural stem cells (NSCs) within the cerebral cortex, but the long-term impact of the complete loss of *Nfix* is difficult to assess, as homozygotes die at weaning [9,15]. Interestingly, NFIX is expressed by neurons in each of the six layers of the cortical plate of the adult mouse neocortex [16], however, the role of NFIX in these mature neuronal populations has not been investigated. Recently, we have shown that NFIX is a crucial mediator within the adult NSC

populations of the hippocampus [17] and ventricular-subventricular zone [18] of the mature mouse brain. In contrast, *Nfix* heterozygous (*Nfix*$^{+/-}$) mice survive until adulthood [9,11] making them an ideal model to investigate brain size and connectivity as a proxy for Malan syndrome. We have previously shown that adult *Nfix*$^{+/-}$ mice exhibit abnormal hippocampal morphology, and have deficiencies in the Morris water maze, a hippocampal-dependent learning and memory task [10]. However, a deeper investigation of brain structure, connectivity and function has yet to be performed on *Nfix*$^{+/-}$ animals. Here, we performed magnetic resonance imaging (MRI), immunohistochemistry and analysis of cortically-controlled behavior in adult *Nfix*$^{+/-}$ mice. We reveal that *Nfix*$^{+/-}$ mice exhibit megalencephaly, as well as abnormal connectivity within major cortical regions. Furthermore, these mice exhibit learning and memory impairments, as well as abnormal social behaviors, that are reminiscent of intellectual disability in human patients. Collectively, these data suggest that the macrocephaly exhibited within Malan syndrome likely arises from megalencephaly, as well as providing insights into the structural and behavioral correlates underlying the intellectual disability of these patients.

2. Materials and methods

2.1. Animals

All experiments conformed to The University of Queensland's Animal Welfare Unit guidelines for animal use in research (AEC approval number: QBI383/16). Additionally, all work was carried in accordance to the Australian Code of Practice for the Care and Use of Animals for Scientific Purposes and the University of Queensland's Institutional Biosafety committee. Mice were maintained on a C57BL/6 J background. Experiments were conducted using adult (11–13 weeks) *Nfix* heterozygous mice (*Nfix*$^{+/-}$) and wildtype (*Nfix*$^{+/+}$) littermate mice as controls. All animals were genotyped as described previously [9].

2.2. Magnetic resonance imaging

For volumetric and diffusion MRI analyses, adult *Nfix*$^{+/+}$ (male = 5, female = 4) and *Nfix*$^{+/-}$ (male = 4, female = 7) brains were used. Mice were anesthetized with lethabarb (VIRBAC PTY) and perfused transcardially with 0.1 M phosphate-buffered saline (PBS), followed by 4% (*w/v*) paraformaldehyde (pH 7.4; Sigma-Aldrich) in PBS. Brains were removed from the skull and post-fixed in 4% PFA for 24 h. Before MRI scanning, the brains were washed in 0.1 M PBS with 0.2% *v/v* gadopentetate dimeglumine (Magnevist, Bayer, Leverkusen) for four days [19]. MRI data were acquired using a 16.4 T vertical bore microimaging system (Bruker Biospin, Rheinstetten; ParaVision v6.01) equipped with Micro2.5 imaging gradient and a 15 mm linear surface acoustic wave coil (M2M, Brisbane, Australia). Three-dimensional (3D) T_1/T_2*-weighted FLASH structural images were acquired using a gradient echo imaging sequence with the following parameters: repetition time (TR) = 50 ms, echo time (TE) = 12 ms, bandwidth = 50 kHz, field of view (FOV) = 19.6 × 11.4 × 8.4 mm and matrix size = 654 × 380 × 280, which results in 30 μm isotropic image resolution, with the acquisition time of 30 mins. 3D diffusion-weighted images (DWI) data were acquired using a Stejskal-Tanner DWI spin-echo sequence with TR = 200 ms, TE = 23 ms, δ/Δ = 2.5/12 ms, bandwidth = 50 kHz, FOV = 19.6 × 11.4 × 8.4 mm and matrix size = 196 × 114 × 84, image resolution = 100 μm, 30 direction diffusion encoding with b-value = 5000 s/mm^2, two b = 0 images, with the acquisition time of 17 h. DWI datasets were zero-filled by a factor of 1.5 in all dimensions prior to Fourier transform to improve fiber tracking [20].

To perform volumetric analyses, the Brookhaven National Laboratory (BNL) 3D MRI C57BL/6 J adult mouse brain atlas [21] was registered to the FLASH images using FMRIB Software Library's linear and non-linear registration (FLIRT and FNIRT, fsl.fmrib.ox.ac.uk). Model-based

segmentation of 20 brain regions was performed on each sample and their volumes were measured using ITK-SNAP (www.itksnap.org/). To analyze the diffusion MRI data, the intensity of the DWI datasets were first bias corrected using ANTs N4BiasFieldCorrection and processed using MRtrix3 software (www.mrtrix.org). Fiber orientation distribution (FOD) was reconstructed using constrained spherical deconvolution (CSD) method, and probabilistic tractography was performed using iFOD2 algorithm. Tractography was performed for specific major white matter tracts, and for the whole brain for the structural connectome analyses. Firstly, the seeding regions of interest (ROIs) were manually drawn in the midsagittal and coronal sections of the color vector map, and fiber tracks were generated for the corpus callosum, hippocampal commissure, and anterior commissure at 100 seeds per voxel. From these structures parametric maps, including tract density imaging (TDI, which measures number of tracts within a voxel unit) [22] and diffusion-tensor MRI (DTMRI) metrics, including fractional anisotropy (which measures the microstructural integrity of axonal tracts), and mean, radial and axial diffusivities (which measures the overall water motility, and in the perpendicular and parallel orientations to axonal bundles, respectively) [23] were calculated for each structure and compared between wildtype and $Nfix^{+/-}$ brains. To perform structural connectome analyses, whole-brain probabilistic tractography was generated using 10 seeds per voxel. The modified Centre for Advanced Imaging (CAI)-John Hopkins MRI atlas [24] was used to segment the whole brain tractography into a connectivity matrix comprising of 100 nodes. The degree of a node in a network corresponds to the number of connections a node has with other nodes. The Network Based Statistic (NBS) toolbox [25] was used to detect changes in the brain connectivity network between wildtype and $Nfix^{+/-}$ mouse brains. NBS results was examined using a range of primary thresholds ($t = 2.5$ to 3.5) to avoid false positive and bias from using a single threshold [24]. The final brain connectivity changes were presented using the results calculated at $t = 3.5$ based on the highest statistical significance (the lowest family wise error rate (FWER)-corrected p-value of any components). No differences in the volumetric and tractography analyses were found between genders within each genotype in our dataset, hence results shown (Table 1, Fig. 2, Fig. 3 and Fig. 4) include combined genders.

2.3. Immunohistochemistry

Animals were perfused as described above (2.2) and brains were stored in 0.1 M PBS at 4 °C until required. For all histological experiments, brains were post-fixed for 48–72 h before being embedded in 3% noble agar (BD Biosciences) and sectioned coronally at 50 μm using a vibratome (Leica). Sections ($n = 3$) from comparable positions along the rostral-caudal axis of the brain were used for each genotype ($n = 3$). For hematoxylin staining, sections were rehydrated in tap water and incubated in Mayer's Hematoxylin (Sigma-Aldrich, USA) solution for 2 and half minutes. The sections were washed for 1 min with tap water before being dehydrated in an ethanol-xylene series and cover-slipped using DPX mounting medium (Ajax Finechem). An Aperio slide scanner using Imagescope (Lecia Biosystems) at 20× magnification was used for all brightfield images. Immunofluorescence labelling was performed as previously described [26]. Briefly, sections were mounted on slides before heat-mediated antigen retrieval was performed in a 10 mM sodium-citrate solution (pH 6.0) at 95 °C for 15 min. Sections were incubated for 2 h in a blocking solution [2% vol/vol normal donkey serum (Vector Laboratories) with 0.2% vol/vol Triton-X 100 in PBS] containing donkey serum. Primary antibodies diluted in blocking solution were applied to sections and incubated overnight at 4 °C. The following primary antibodies were used: anti-Ctip2 (1:400, Abcam #ab18465), anti-Satb2 (1:500, Abcam #ab51502), anti-Olig2 (1/400, Abcam #ab9610), anti PDGFRα (1/200, R&D Systems #AF1062), and anti-S100β (1/400, Abcam #ab66028). Following overnight incubation, corresponding secondary antibodies (Alexa Flour488 and Cy3 raised in donkey) were applied to sections for 2 h. Sections were counter-stained with Hoechst (Thermo Fisher) and cover-slipped using fluorescent mounting medium (DAKO). The following cellular populations were analyzed: upper (II, III, IV) layer neurons (Satb2+/Ctip2-), deeper (V, VI) layer neurons (Satb2-/Ctip2+), astrocytes (S100β+), oligodendrocyte precursors (Olig2+/PDGFRα-), and mature oligodendrocytes (Olig2+/PDGFRα+). Immunofluorescence labelled sections were imaged at 10× magnification on a Diskovery spinning disk confocal microscope using NIS Elements (Nikon19) and Andor iXon888 EMCCD camera at a depth of 15 μm and Z-step size of 2.5 μm. Low magnification fluorescent images represent composite images of

Table 1
Volume changes in the $Nfix^{+/-}$ adult mouse brain.

Structure	Absolute volume (mm³) (mean ± SD)			$Nfix^{+/-}$ % increase
	$Nfix^{+/+}$	$Nfix^{+/-}$	p-value	
Total brain	457.75 ± 20.63	532.34 ± 22.61	<0.0001	16.29%
Corpus callosum and external capsule	15.94 ± 1.64	20.00 ± 1.24	<0.0001	25.46%
Neocortex	139.29 ± 9.75	171.49 ± 8.86	<0.0001	23.11%
Anterior commissure	1.14 ± 0.07	1.34 ± 0.11	<0.001	17.52%
Basal forebrain septum	13.59 ± 0.79	15.91 ± 0.75	<0.0001	17.00%
Amygdala	12.86 ± 0.76	15.03 ± 0.87	<0.0001	16.88%
Caudate putamen	27.31 ± 1.22	31.87 ± 1.51	<0.0001	16.66%
Hippocampus	26.53 ± 1.49	30.84 ± 1.67	<0.0001	16.24%
Globus pallidus	3.23 ± 0.12	3.74 ± 0.21	<0.0001	15.78%
Ventricles	1.57 ± 0.12	1.81 ± 0.10	<0.001	15.22%
Hypothalamus	12.51 ± 0.77	14.31 ± 1.07	<0.001	14.40%
Internal capsule	2.70 ± 0.13	3.08 ± 0.13	<0.0001	13.93%
Thalamus	26.54 ± 1.23	30.22 ± 1.04	<0.001	13.88%
Cerebellum	51.83 ± 3.26	58.97 ± 2.11	<0.0001	13.77%
Fimbria	2.77 ± 0.18	3.10 ± 0.17	<0.001	11.97%
Superior colliculi	8.86 ± 0.39	9.86 ± 0.58	<0.001	11.32%
Inferior colliculi	6.40 ± 0.45	7.09 ± 1.02	ns.	10.75%
Brain stem	54.87 ± 3.07	58.89 ± 4.66	<0.05	7.34%
Rest of midbrain	12.25 ± 0.57	13.49 ± 0.69	<0.001	10.16%
Central gray	4.27 ± 0.18	4.60 ± 0.24	<0.05	7.93%
Olfactory bulb	25.06 ± 1.18	26.02 ± 4.71	<0.001	3.80%

The BNL C57BL/6 J adult mouse brain atlas was used to perform model-based segmentation of 20 brain sub regions in wildtype ($Nfix^{+/+}$, n = 9) and heterozygous ($Nfix^{+/-}$, n = 11) mice. All sub regions within the $Nfix^{+/-}$ adult mice, except for the inferior colliculi, showed significantly increased absolute volumes. The percentage of $Nfix^{+/-}$ total brain and all sub regions was increased compared to wildtypes. Statistical analyses performed using Student's t-test and multiple comparisons were adjusted using the Bonferroni-Dunn correction method.

the whole 15 μm stack, whereas high-magnification images represent a single 2.5 μm optical slice. All histological images were analyzed in Fiji (ImageJ, open-source). Neocortical cell counts were performed in a counting window of 270 μm width by 1600 μm length by 15 μm depth, using the Allen Brain Atlas (http://atlas.brain-map.org/atlas) as a guide. All measurements and cell counts were performed along the rostral-caudal axis blind to the genotype. For Di-I labelling, 3-week old control ($n = 5$) and $Nfix^{+/-}$ mouse (n = 5) were transcardially perfused with 4% PFA and post-fixed in 4% PFA for 24 h before extracting brains. Brains were hemisected using sharp blade and DiI crystal was inserted into the anterior commissure using the fornix as a guide. Brains were incubated in 4% PFA at 37 °C for 4 months before being sectioned coronally at 50 μm using a vibratome and imaged using the Discovery spinning disk confocal microscope.

2.4. Behavioral assays

Littermates of the same gender were raised together in boxes containing 2–5 mice regardless of their genotype. Mice were subjected to the least stressful test (3-chambered sociability) first before the most stressful test (active place avoidance) with a 2-day break between experiments. All data were acquired using Ethovision™XT (Noldus Information Technology, NLD) tracking software and experiments were performed blind to the genotype of mice. A modified 3-chambered sociability test apparatus [27] was used to examine social behavior, specifically social approach behavior in Trial 1 and preference for social novelty in Trial 2. Adult mice included 29 $Nfix^{+/+}$ (male = 18, female = 11) mice and 32 $Nfix^{+/-}$ (male = 21, female = 11) mice. Briefly, the test mouse was placed in the center of a 3-chambered social interaction apparatus to habituate for 5 min. In Trial 1, the test mouse was confined to the central chamber using dividers and the first conspecific mouse of the same-sex and size was placed centrally in either the left or right chamber within a wire framed steel cage. The dividers were removed and the test mouse moved freely between the three chambers for 5 min. In trial 2, the test mouse was again confined to the central chamber and a second novel mouse was placed in the remaining wired framed steel cage. The dividers were removed and the test mouse moved freely between the three chambers for a further 5 min. The amount of time spent in close proximity to the conspecific mouse (interaction zone set to 6 cm radius) was recorded for each test mouse over each trial and during habituation. The APA task was used to assess spatial navigation, learning and memory [28], and was performed as described previously [29]. Adult mice included 26 $Nfix^{+/+}$ (male = 15, female = 11) mice and 28 $Nfix^{+/-}$ (male = 15, female = 13) mice. Briefly, the test mouse was placed onto a slowly rotating (clockwise at 1 rotation per minute) platform arena situated within a room marked by four visual cues on each wall. When the animal entered a fixed shock zone within the arena, an electric shock (0.5 milliamps charge) was released at 15 milliseconds intervals until mouse left the shock zone. Prior to testing, the test mouse first underwent habituation, where it explored the arena for 5 min without (inactive) electric shocks. The following day began the first of 5 consecutive days in which the mouse was placed on the rotating platform for 10 min with active electric shocks. Measurements taken include, number of shocks received, latency to first and second entrance into the zone, maximum time the mouse avoided the zone, average speed, and total distance travelled. The time to the second entrance was calculated from the start of the experiment until the time of the second entrance of a mouse to the shock zone. Analysis of each gender (Fig. S4) within the 3-chambered sociability and APA task revealed no differences between genotypes in all measurements taken, hence, all analyses in Fig. 5 and Fig. 6 were pooled by gender.

2.5. Statistical analyses

Statistical analyses were performed using GraphPad Prism 7 (GraphPad Software, La Jolla California USA). Student's t-tests were used when comparing two groups. Two-way ANOVA was performed involving two independent variables, with repeated measures if applicable. Multiple comparisons were adjusted using the Bonferroni-Dunn correction method. Statistical significance was established at a p-value of <0.05. Error bars on graphs represent standard error of the mean (SEM).

3. Results

3.1. $Nfix^{+/-}$ adult mice exhibit increased brain volume

Given that Malan syndrome patients have relatively normal brain structure [5], we hypothesized that the macrocephalic phenotype present in Malan syndrome patients is due to an expansion of brain size. To address this, we performed in-depth neuroimaging and histological analyses using adult $Nfix^{+/-}$ mice as a model. Firstly, using high-resolution gradient echo (T_1/T_2*-weighted) imaging at a resolution of 30 μm, we examined the volumetric differences of 20 sub regions of the brain between adult $Nfix^{+/-}$ and wildtype mice (Table 1). Total brain volume was significantly ($t_{17} = 7.36$, $p < .0001$) increased in $Nfix^{+/-}$ (532.34 ± 22.61) mice compared to wildtypes (457.75 ± 20.63). Partitioning of the brain into sub regions further indicated that the volumes of 19 out of 20 regions of the brain in $Nfix^{+/-}$ mice were significantly increased (Table 1). Further analysis showed that the three largest volume increases in the heterozygous brain included the corpus callosum (25.46%), neocortex (23.11%), and anterior commissure (17.52%). Interestingly, the percentage of each sub region to the total brain volume was very similar between $Nfix^{+/-}$ and wildtypes (data not shown), indicating that the expansion of total brain volume is due to a proportionate increase of all sub regions throughout the brain. This is consistent with expression data in mice showing that NFIX is expressed in proliferative zones throughout the developing embryonic neuroaxis, including the dorsal and ventral telencephalon (Fig. S1), as well as the developing brain stem [9,11,15,30]. Taken together, these data demonstrate that $Nfix^{+/-}$ mice have megalencephaly.

3.2. Expansion of cortical layers within the neocortex of $Nfix^{+/-}$ adult mice

Megalencephaly can be characterized by excessive neuronal and/or glia production, or abnormal migration leading to enlarged cerebral growth [6–8]. Therefore, we next investigated potential causes that could underlie megalencephaly in these $Nfix$ heterozygotes. Focusing on the neocortex, we compared the thickness of the cortical plate in adult $Nfix^{+/-}$ and wildtype mice using hematoxylin stained coronal sections at rostral and caudal levels. On rostral sections, measurements were taken at the cingulate cortex and rostral somatosensory cortex, while caudal sections were used to measure the cortical plate thickness within the retrosplenial cortex and the caudal somatosensory cortex (Fig. 1a-b). The thickness of the $Nfix^{+/-}$ neocortex was significantly larger in comparison to wildtypes (Fig. 1c-d). The cingulate cortex increased by 25.02%, ($t_6 = 4.342$, $p = .004$), rostral somatosensory cortex by 19.02% ($t_6 = 2.86$, $p = .023$), caudal somatosensory cortex by 29.49% ($t_4 = 3.203$, $p = .03$), and retrosplenial cortex by 27.79% ($t_4 = 5.506$, $p = .005$).

Given these findings, we hypothesized that the increased thickness of the cortical plate in $Nfix$ heterozygotes could arise from elevated numbers of neurons and glia, which are the post-mitotic progeny of cortical NSCs [31]. To test this, we performed co-immunofluorescence labelling using cell-specific markers on adult $Nfix^{+/-}$ and wildtype coronal sections. We quantified upper (II, III, IV) layer neurons using special AT-rich sequence-binding protein 2 (Satb2) antibody [32], deep (VI and V) cortical neurons using chicken ovalbumin upstream promoter transcription factor-interacting protein 2 (Ctip2) antibody [33], astrocytes using S100 calcium-binding protein β (S100β) [34], and precursor oligodendrocytes and myelinated oligodendrocytes using oligodendrocyte transcription factor 2 (Olig2) [35], and platelet-

derived growth factor receptor α (PDGFRα) [36] antibodies, respectively. Notably, there was no obvious disruption of cortical lamination of the neuronal populations within each layer of the $Nfix^{+/-}$ neocortex compared to wildtypes (Fig. 1e-f). Quantification within the retrosplenial and somatosensory cortex (Fig. 1g-h) revealed significant increase in Satb2+ upper layer neurons/μm^3 (retrosplenial: $t_5 = 3.348$, $p = .02$; somatosensory: $t_5 = 6.458$, $p = .001$) and Ctip2+ deeper layer neurons/μm^3 (retrosplenial: $t_5 = 3.099$, $p = .027$; somatosensory: $t_5 = 5.02$, $p = .004$) in the $Nfix^{+/-}$ cortex. Moreover, quantification of glial cells (Fig. S2) showed increased S100β + astrocytes/μm^3 (somatosensory: $t_4 = 3.656$, $p = .022$) and Olig2+ oligodendrocytes/μm^3 (retrosplenial: $t_4 = 3.157$, $p = .034$; somatosensory: $t_4 = 3.391$, $p = .028$) PDGFRα+ oligodendrocytes/μm^3 (retrosplenial: $t_4 = 4.534$, $p = .011$; somatosensory: $t_4 = 7.284$, $p = .002$). The density of all cell-types was not significantly different between heterozygous and wildtype cortices (data not shown), indicating that the expansion of cortical thickness is due to an increase in overall cell number while maintaining a normal cellular distribution. Additionally, there were no significant changes in the ratio of the thickness of layers II-IV over layers V-VI between the genotypes in any of the cortical regions analyzed. Collectively, the MRI volumetric and immunohistochemical analyses reveal that $Nfix$ heterozygosity culminates in elevated neural and glial cell number within the adult neocortex, ultimately leading to megalencephaly within these animals.

3.3. $Nfix^{+/-}$ adult mice have aberrant microstructure of major forebrain commissure tracts

To date, neuroimaging analysis of Malan syndrome patients has been very limited, and thus, the consequence of $NFIX$ haploinsufficiency with relation to brain connectivity remains unknown. While Malan syndrome patients display hypoplasia of the corpus callosum [5], the extent of axonal disruption and subsequent structural organization has not been studied. To address this, we performed diffusion tensor magnetic resonance imaging (DTMRI) and tractography-based analyses on the three major forebrain commissures, the corpus callosum, the hippocampal commissure and the anterior commissure, of adult $Nfix^{+/+}$ and $Nfix^{+/-}$ mice. In wildtype mouse brains, all three commissures revealed well-defined white matter tract bundles and high fractional anisotropy (Fig. 2a-l). In contrast, the commissures in $Nfix^{+/-}$ mice revealed significantly reduced fractional anisotropy (Fig. 2m) within the corpus callosum ($t_{18} = 2.28$, $p = .035$), the hippocampal commissure ($t_{18} = 3.1$, $p = .006$), and the anterior commissure ($t_{18} = 3.796$, $p = .001$). Furthermore, compared to wildtypes, all three $Nfix^{+/-}$ forebrain commissures (corpus callosum: $t_{18} = 2.414$, $p = .02$; hippocampal commissure: $t_{18} = 3.901$, $p = .001$; anterior commissure: $t_{18} = 4.108$, $p = .0007$) had significantly less axial diffusivity (Fig. 2n), while the $Nfix^{+/-}$ anterior commissure ($t_{18} = 3.22$, $p = .005$) also exhibited significantly reduced radial diffusivity (Fig. 2o). Taken together, these data demonstrate that the forebrain commissures had loss of microstructural integrity and reduced directional coherence, indicative of abnormal fanning and bending of white matter tracts. Directionality maps of $Nfix^{+/-}$ brains revealed that the fiber tracts of the major forebrain commissures were indeed aberrantly dispersed (Fig. 3a-l). This was most prominent in the anterior commissure (Fig. 3i-l), which showed an abnormally high number of tracts in the dorsal-ventral direction compared to wildtypes. The tract density intensity of the $Nfix^{+/-}$ hippocampal commissure ($t_{18} = 3.086$, $p = .006$) and anterior commissure

($t_{18} = 3.997$, $p < .0008$) were also significantly decreased compared to wildtypes (Fig. 3m), indicating that the axonal tracts within these structures were less densely packed.

To validate whether the abnormal fiber tracts in $Nfix^{+/-}$ mice identified by DTMRI tractography were recapitulated in vivo, we performed fluorescent DiI labelling on the most severely affected white matter tract, the anterior commissure. Results showed that the DiI had diffused in a tight lateral direction within the anterior commissure of wildtype brains (Fig. S3a), while the DiI diffused largely in a dorsal-ventral direction in the $Nfix^{+/-}$ anterior commissure (Fig. S3b). Hence, the axonal tract diffusivity of the $Nfix^{+/-}$ anterior commissure in vivo supports the DTMRI tractography data. Taken together, these data demonstrate that the enlarged $Nfix^{+/-}$ brains display aberrant microstructural organization of the major forebrain commissures.

3.4. Abnormal structural connectome of the $Nfix^{+/-}$ adult mouse brain

The structural abnormalities within the forebrain commissures of $Nfix^{+/-}$ mice identified with DTMRI tractography led us to perform a more comprehensive analysis of brain connectivity. To do this we constructed the structural connectome of 100 brain areas (nodes) throughout the whole brain of $Nfix^{+/-}$ and wildtype mice. Using the NBS toolbox, we performed connection-wise comparisons, which compares each connection of the structural connectome, to identify individual nodes that were significantly altered (either increased or decreased connectivity) in the $Nfix^{+/-}$ brain compared to wildtypes. The degree of change in a node corresponds to the number of different connections made with that node. The connection-wise comparisons revealed two main abnormal patterns. Firstly, $Nfix^{+/-}$ brains displayed significantly increased connections (Fig. 4a-b) within the limbic system, including the hypothalamus (degree 8), amygdala (degree 2–6), hippocampus (degree 3), and thalamus (degree 1–4), as well as regions directly associated with these brain areas such as the piriform cortex (degree 2). Notably, the anterior commissure (degree 5) also had significantly increased connections, consistent with our tractography findings. In contrast, $Nfix^{+/-}$ brains exhibited significantly reduced connections (Fig. 4c-d) within the motor cortices (degree 1–2) primarily in the right hemisphere and the prefrontal cortex (degree 2–4). Additionally, a few sub regions of the limbic system (degree 1–4) also displayed decreased connections linked with the prefrontal and motor cortices. Together, these data indicate that heterozygosity of $Nfix$ culminates in abnormal connectivity between many crucial brain regions.

3.5. Adult $Nfix^{+/-}$ animals exhibit learning and memory impairments

Given that Malan syndrome patients display intellectual disability [1,5] and that our data shows $Nfix^{+/-}$ brains have significant abnormal cortical connectivity (Fig. 4), we posited that these animals might exhibit deficits in cortically-controlled behavior. To test this, we examined spatial learning and memory function using the APA task, which involves the hippocampal-prefrontal cortex circuitry and is considered a rodent model of higher cognitive function in humans [28,37]. The APA task requires rodents to learn and avoid the location of a stationary shock zone based on visual cues (Fig. 5a) over five consecutive days of testing (with shocks) following a day of habituation (no shocks) to the environment. During habituation, and over the testing paradigm, there were no significant differences in the total distance travelled between $Nfix^{+/-}$ mice and controls (Fig. S4a-c), thus, indicating normal

Fig. 1. $Nfix^{+/-}$ mice have expanded cerebral cortices and increased number of cortical neurons. Hematoxylin stained coronal sections of adult (**a**) $Nfix^{+/+}$ control ($n = 4$) and (**b**) $Nfix^{+/-}$ ($n = 4$) brains shown at low magnification (caudal section as representative), panels (**a′**) and (**b′**) at higher magnification. Thickness measurements (black lines in **a′** and **b′**) were taken of the cingulate cortex and rostral somatosensory cortex using rostral sections, and retrosplenial cortex and caudal somatosensory cortex on caudal sections. (**c, d**) The thickness of the cingulate, retrosplenial, and somatosensory cortex of $Nfix^{+/-}$ mice were significantly larger than $Nfix^{+/+}$ animals. (**e, f**) Co-immunofluorescence was performed on coronal caudal sections ($n = 3$ per genotype) using antibodies against Satb2 to identify cortical neurons in upper (II, III, IV) layers and Ctip2 to label neurons in deeper (V, VI) layer neurons. Cell counts were performed in a window of 1000 μm width by 6000 μm length by 15 μm depth within the retrosplenial cortex (**e′, f′**) and somatosensory cortex (**e″, f″**). Results showed significant increases in Satb2+ upper and Ctip2+ deeper cortical neuron number in both the retrosplenial and somatosensory cortices of $Nfix^{+/-}$ mice (**g, h**). Data are represented as mean ± SEM. (ns) not significant, *$p < .05$; **$p < .01$, t-test. Scale bars: (**b**) = 1 mm, (**b′**) = 500 μm, (**f**) = 250 μm, (**f″**) = 100 μm.
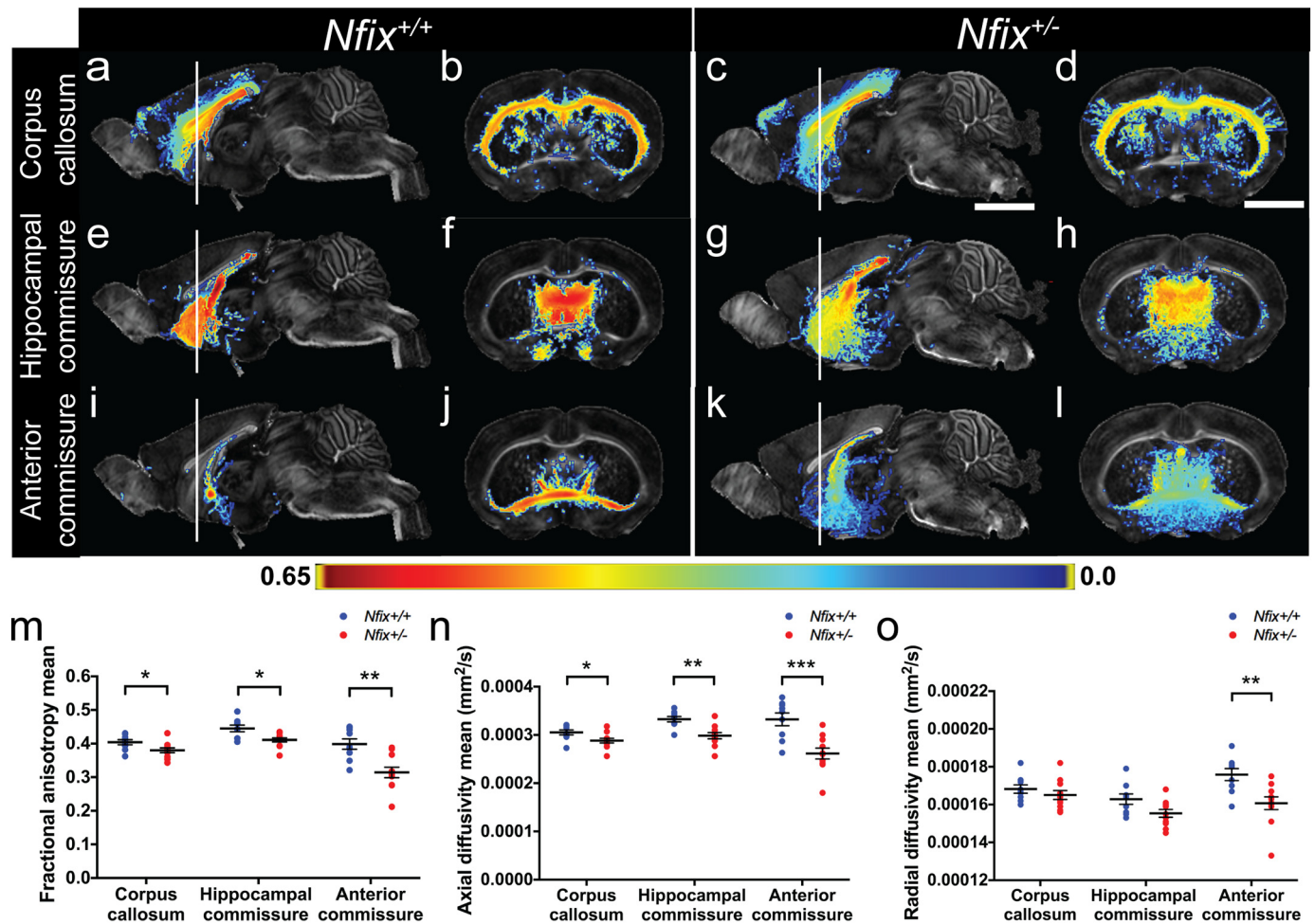
Fig. 2. $Nfix^{+/-}$ mice display a loss of axonal tract integrity within the major forebrain commissures. Fractional anisotropy heat maps of the corpus callosum, hippocampal commissure and anterior commissure of adult (**a, b, e, f, i, j**) $Nfix^{+/+}$ control ($n = 9$) and (**c, d, g, h, k, l**) $Nfix^{+/-}$ mice ($n = 11$) brains shown on mid-sagittal and coronal planes respectively. (**m**) Fractional anisotropy of $Nfix^{+/-}$ corpus callosum, hippocampal commissure, and anterior commissure were significantly reduced compared to controls. (**n**) All three tracts in $Nfix^{+/-}$ had significantly less axial diffusivity, which measures water motility in the parallel orientation to axonal bundles, than controls. (**o**) While only the anterior commissure had significantly reduced radial diffusivity in $Nfix^{+/-}$ brains, which measures water motility in the perpendicular orientation to axonal bundles. Data are represented as mean ± SEM. (ns) not significant, *$p < .05$; **$p < .01$; ***$p < .001$, t-test. Scale bar: (**c, d**) = 5 mm.

locomotor function, exploratory behavior, and task participation, which are in accordance with previous SHIRPA and locomotor behavior assessment of adult $Nfix^{+/-}$ animals [10]. Crucially, however, $Nfix^{+/-}$ animals demonstrated significant learning and memory deficits compared to wildtypes (Fig. 5b). $Nfix^{+/-}$ mice received significantly more shocks than wildtypes ($F_{1, 52} = 20.21$) on days 3 ($p = .001$), 4 ($p = .017$), and day 5 ($p = .048$) (Fig. 5c). The time to first shock measurement on days 2 to 5 is indicative of long-term memory function [38]. In comparison to wildtypes, $Nfix^{+/-}$ mice received their first shock significantly earlier ($F_{1, 52} = 8.584$) on days 4 ($p = .024$) and 5 ($p = .0001$), thus indicating relatively poor long-term memory (Fig. 5d). Short-term memory can also be investigated in this task via an analysis of the latency to the second entry to the shock zone [38]. Once again, the latency to the second entry ($F_{1, 52} = 9.986$) was shorter on days 4 ($p = .018$) and 5 ($p = .005$) in $Nfix^{+/-}$ mice compared to wildtypes (Fig. 5e). The maximum time $Nfix$ heterozygotes avoided the shock zone was also shorter than wildtypes (Fig. 5f). Interestingly, while $Nfix^{+/-}$ mice showed significantly reduced learning and memory performance compared to wildtypes (Fig. 4d-f), intra-genotype analyses revealed that neither wildtype or heterozygous mice fully learned the task, as the total number of shocks each cohort received was not significantly different between day 1 and day 5 of the test (Fig. S4d). However, intra-genotype analyses of different aspects of the test, including time to first shock, time to second entry, and maximum time between

shocks revealed that both wildtype and heterozygous animals do show improved learning and memory at day 5 compared to day 1 (Fig. S4e-g). This suggests that $Nfix^{+/-}$ mice can learn facets of this task, albeit their performance is reduced in comparison to wildtypes. There were no differences between genders per genotype in all analyses (Fig. S4 h-i). Collectively, these results demonstrate that $Nfix^{+/-}$ mice exhibit significant spatial learning and memory impairment in adulthood, and thus, may provide a useful model of intellectual disability in Malan syndrome patients.

3.6. Adult $Nfix^{+/-}$ animals display abnormal social behavior

Malan syndrome patients exhibit autistic-like traits and elevated anxiety [1,3,5]. A principal diagnostic criterion of autism is deficits in social interaction [39]. Although autism is a human disorder, rodents have been extensively used to model some of its characteristic phenotypes, including social behavior [40]. Additionally, social behavior is known to involve the prefrontal cortex [41] and we have demonstrated that $Nfix^{+/-}$ mice have abnormal connectivity within sub regions of the frontal cortex (Fig. 4). Therefore, we next examined the social behavior of $Nfix^{+/-}$ mice to model autistic-like traits in Malan syndrome. To do this, we used the 3-chambered sociability task, which has been widely used to model aspects of social interaction behavior in rodent models [27,42,43]. The task involves the test mouse being placed within the
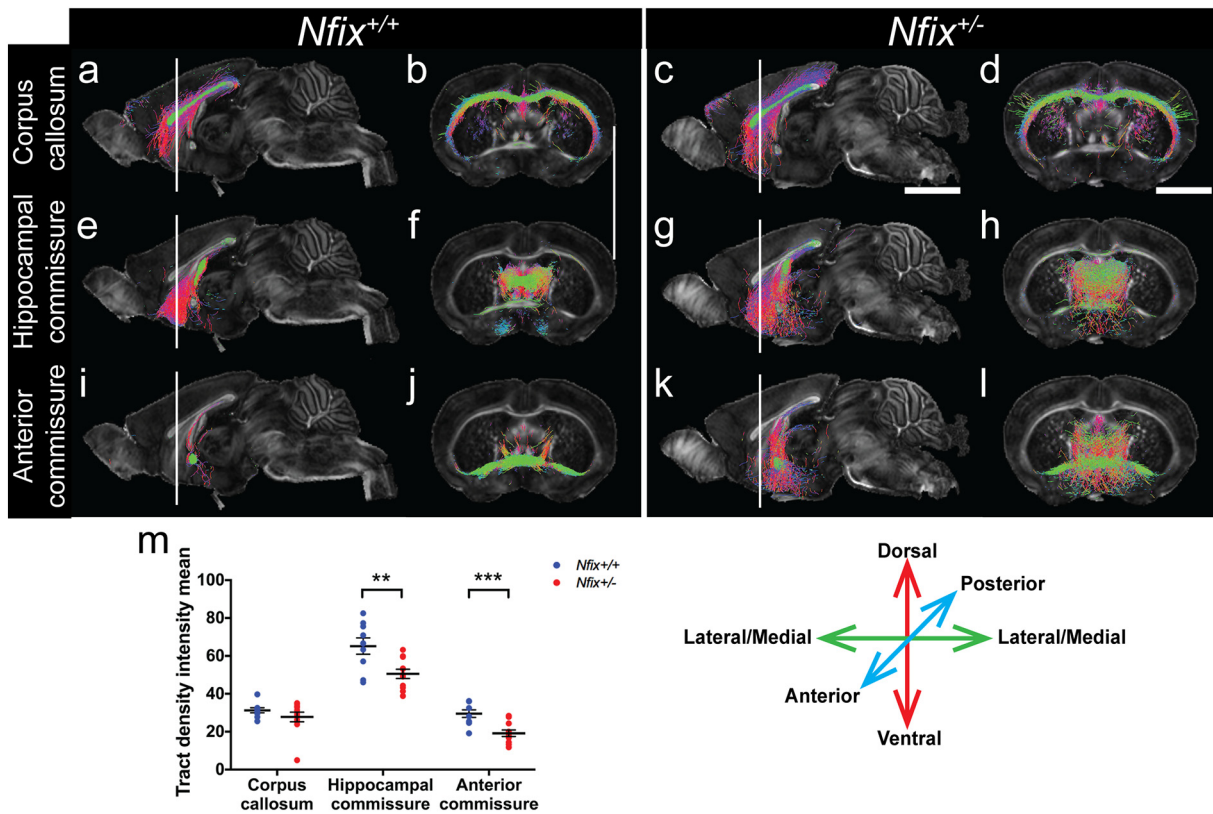
Fig. 3. $Nfix^{+/-}$ mice display aberrant directionality of axonal tracts within the major forebrain commissures. Directionality maps of the corpus callosum, hippocampal commissure and anterior commissure of adult (**a, b, e, f, i, j**) $Nfix^{+/+}$ control (n = 9) and (**c, d, g, h, k, l**) $Nfix^{+/-}$ mice (n = 11) brains shown on mid-sagittal and coronal planes respectively. (**m**) Tract density intensity of $Nfix^{+/-}$ corpus callosum, hippocampal commissure, and anterior commissure were significantly decreased compared to controls. The color code (key) indicates the direction of axon fiber tracts (red, dorsal-ventral; green, lateral-medial; blue, rostro-caudal). Data are represented as mean ± SEM. (ns) not significant, **$p < .01$; ***$p < .001$, t-test. Scale bar: (**c, d**) = 5 mm.

central chamber of a three chamber setup. The test mouse is allowed to interact with two unfamiliar mice (same sex and size), called conspecifics, in two separate trials where the first examines social approach behavior and the second trial assesses preference for social novelty [43]. During the habituation period of the task, where the test mouse was allowed to explore all three empty chambers, $Nfix^{+/-}$ mice and wildtypes showed no preference for either the left or the right chamber (Fig. S4j-l), indicating comparable exploratory behavior. Furthermore, there were no differences between genders per genotype for each trial (Fig. S4 m).

In trial 1, the test mouse was allowed to explore and initiate social contact with the first conspecific mouse held inside a wired cage, or an identical empty wired cage (Fig. 6a). We first performed comparisons within genotypes and found that throughout the total 5-min period of trial 1 ($F_{1, 118} = 14.67$; Fig. 6b-c) wildtype animals spent significantly ($p = .0003$) more time with the first conspecific mouse compared to the empty chamber. In contrast, $Nfix^{+/-}$ mice demonstrated no significant ($p = .311$) differences in the time spent between the first conspecific mouse and the empty chamber. However, within the first minute of trial 1 ($F_{1, 104} = 32.86$; Fig. 6d), both wildtype ($p = .0002$) and $Nfix^{+/-}$ mice ($p = .0002$) interacted with the first conspecific mouse significantly longer than the empty chamber. Comparisons between genotypes throughout the total 5-min period ($F_{1, 118} = 0.169$, $p = .682$) and in the first minute ($F_{1, 118} = 1.873$, $p = .174$) of trial 1 revealed that wildtype and heterozygous animals spent a similar amount of time with both the first conspecific mouse and the empty chamber. Together, these data suggest that while $Nfix^{+/-}$ and wildtype animals spent similar amount of time interacting with the unfamiliar mouse, heterozygous mice displayed no overall social preference for the unfamiliar mouse over an empty chamber.

In trial 2, a novel conspecific mouse was introduced into the previously empty cage (Fig. 6e). During the 5-min period of trial 2 ($F_{1, 114} = 2.393$; Fig. 6f-g), both wildtype ($p = .108$) and $Nfix^{+/-}$ mice ($p > .999$) did not show any differences in the time spent with the novel conspecific mouse compared to the first conspecific mouse. This could be because the first conspecific and novel conspecific mice were littermates with no distinguishing features, and thus, the social novelty may have dissipated quickly. Therefore, we again examined the first minute of introducing the novel conspecific mouse ($F_{1, 102} = 3.314$; Fig. 6h). Interestingly, while the wildtype animals ($p = .013$) spent a significantly longer time with the novel conspecific mouse compared to the first conspecific mouse, $Nfix^{+/-}$ mice ($p > .999$) showed no preference for either the novel or first conspecific mice. Indeed, comparison between genotypes ($F_{1, 102} = 2.782$) revealed that wildtype animals spent significantly ($p = .009$) longer interacting with the novel conspecific mouse than heterozygous animals, while time spent with the first conspecific mouse showed no differences ($p > .999$) between genotypes. Collectively, these data reveal that adult $Nfix^{+/-}$ mice demonstrate abnormal social behavior. Importantly, our investigation of learning and memory function and social behavior indicate that the neuroanatomical changes in $Nfix^{+/-}$ brains likely contribute to deficits in cortically-controlled behavior, which may model intellectual disability featured in Malan syndrome patients.

4. Discussion

$NFIX$ haploinsufficiency has recently been identified as causative for Malan syndrome [1,5]. Other than basic clinical assessment of these patients, our understanding of the developmental processes leading to Malan syndrome is unclear. Germline null $Nfix$ knockout
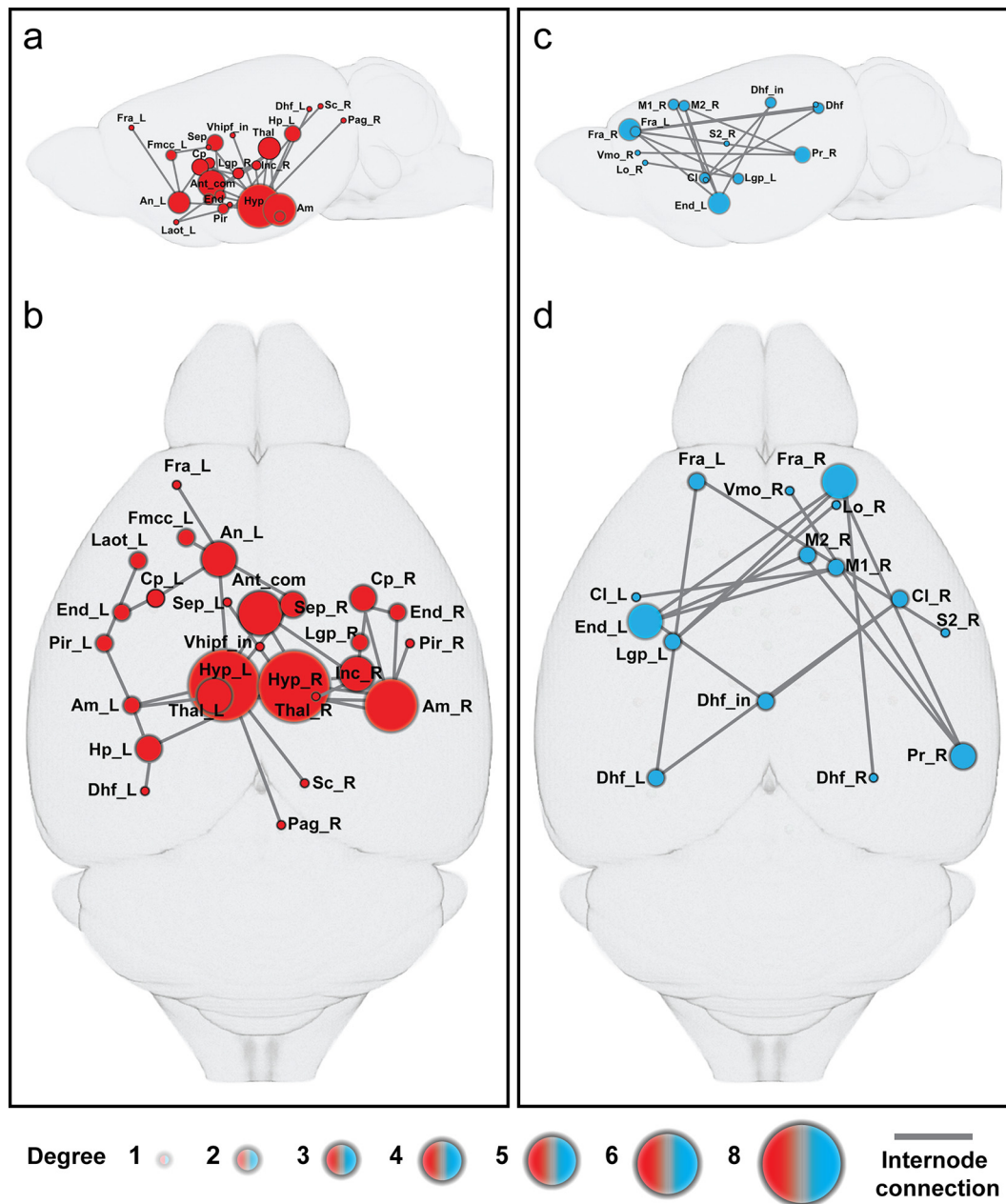
Fig. 4. Structural connectome mapping reveals abnormal inter-nodal connectivity within adult *Nfix*$^{+/-}$ mouse brain. Connection-wise comparisons between *Nfix*$^{+/-}$ brains (n = 11) compared to *Nfix*$^{+/+}$ controls (n = 9) was performed using Network Based Statistic analysis. The extent component (total number of connections) and primary threshold ($t = 3.5$, $p = .0012$) results were used to create an illustration. Brain nodes are represented as circles scaled in size according to the degree of change in a node, which corresponds to the number of different connections made with that node. Abnormal nodes are shown in sagittal (**a, c**) and axial (**b, d**) views. (**a, b**) Nodes that had increased connectivity in *Nfix*$^{+/-}$ compared to controls are depicted in red, (**c, d**) while nodes with decreased connectivity shown in blue. (**a, b**) Compared to controls, *Nfix*$^{+/-}$ brain show significantly increased node degree predominantly within the limbic system, including the hippocampus, hypothalamus, amygdala, and thalamus, as well as regions directly associated with these brain areas. (**c, d**) Meanwhile, *Nfix*$^{+/-}$ brain show significantly decreased node degree within sub regions associated between the prefrontal cortex, motor cortex, and a few limbic structures. All colors and node size are used for demonstration only. Key: Am – amygdala, An – accumbens nucleus, Ant com – anterior commissure, Cl – claustrum, Cp – caudate putamen, Dhf - dorsal hippocampal fissure, End - endopiriform nucleus, Fra - frontal association cortex, Fmcc - forceps minor of the corpus callosum, Hp - hippocampus, Hyp – hypothalamus, Inc. – internal capsule, Lgp – lateral globus pallidus, Laot – lateral olfactory tract, Lo - lateral orbital cortex, M1 - primary motor cortex, M2 - secondary motor cortex, Pag – periaqueductal gray, Pir - piriform nucleus, Sep – septum, Sc - superior colliculus, Thal –thalamus, Vhipf - ventral hippocampal commissure inclusion, Vmo - ventromedial orbital cortex. L - left, R – right.

mice (*Nfix*$^{-/-}$) have several similar characteristics to Malan syndrome patients. For example, Malan syndrome patients have skeletal malformations and visual impairment [5]. Similarly, *Nfix*$^{-/-}$ mice have also been shown to have severe skeletal defects [13,14] and delayed eye development [9]. Malan syndrome patients occasionally have a small callosal body and dilated ventricles [3,5]. These traits are also displayed by *Nfix*$^{-/-}$ mice, which have dysgenesis of the corpus callosum and hydrocephalus [9,13,44]. Previously, *Nfix*$^{-/-}$ mice were

shown to exhibit enlargement of the cingulate cortex at early postnatal ages [9], however, as these animals failed to survive past weaning age further analyses were unable to be performed. Importantly, the underlying causes leading to macrocephaly and the affected cortical regions responsible for intellectual disability in Malan syndrome remain unknown. In the present study, we have used adult *Nfix*$^{+/-}$ mice to model these cortical phenotypes of Malan syndrome. Volumetric MRI and histological analyses demonstrated that *Nfix*$^{+/-}$ mice exhibit
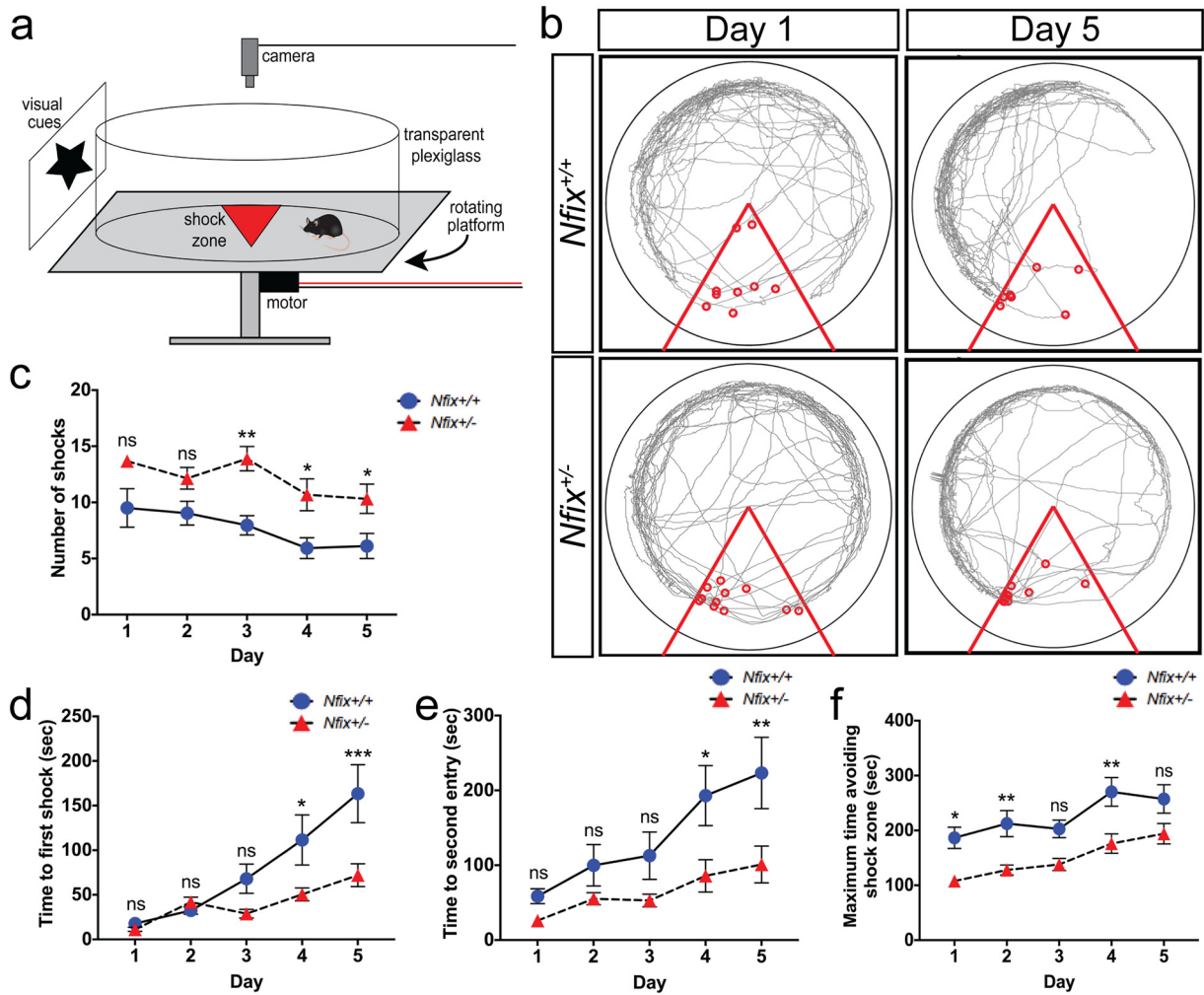
Fig. 5. $Nfix^{+/-}$ mice exhibit learning and memory deficits. (**a**) Adult $Nfix^{+/+}$ control ($n = 26$) and $Nfix^{+/-}$ mice ($n = 28$) performed the active place avoidance task for 10 min each day for 5 days. (**b**) Representative images of Ethovision™XT tracking shown on day 1 and day 5. (**c**) $Nfix^{+/-}$ mice had a consistently higher rate of being shocked compared to controls. (**d**) The time to first shock indicates the mouse remembering to avoid the shock zone at the start of each day. $Nfix^{+/-}$ mice received their first shock significantly earlier compared to controls during the final two days. (**e**) The latency period from the first shock to second entry into shock zone reflects the working memory of mice avoiding the shock zone. Again, during the last two days, $Nfix^{+/-}$ mice were shocked significantly quicker compared to controls. (**f**) The maximum time that control mice avoided the shock zone was consistently longer than the $Nfix^{+/-}$ mice. Data are represented as mean ± SEM. (ns) not significant, $*p < .05$; $**p < .01$; $***p < .001$, two-way ANOVA.

megalencephaly, where the increase in brain volume is underpinned by an overall increase in cell number. Tractography-based analyses of these heterozygous brains further revealed aberrant microstructural integrity of major commissural tracts and critical changes in structural connectivity throughout major cortical regions. Importantly, $Nfix^{+/-}$ mice exhibited learning and memory impairment, as well as abnormal social behavior, reminiscent of intellectual disability and autistic features characterized in Malan syndrome patients. Collectively, the phenotypes of the heterozygous $Nfix$ mouse closely parallels the syndromic features of Malan syndrome patients.

Macrocephaly is a cardinal feature of Malan syndrome; however, the underlying causes leading to enlargement of head circumference is not clear. To date, MRI scans of patients have reported relatively normal brain structure [5]. Could the increased head circumference of these patients be underlined by a global enlargement of brain size? Macrocephaly and megalencephaly can be associated within the same developmental disorder, where cerebral overgrowth can lead to increased head size [6–8]. Additionally, megalencephalic symptoms are syndromic and are often associated with developmental delay, intellectual disabilities, and behavioral problems [7,8], symptoms that are all found in Malan syndrome [5]. To our knowledge, there has not been any specific assessment of brain size within Malan syndrome patients. Here, we reveal that $Nfix$ heterozygosity in mice results in an overall

increase in the number of neurons and glia within the adult neocortex leading to an expansion of cortical thickness (Fig. 1) and thus, culminating in increased neocortical volume (Table 1). The increase in cell number is likely due to the role of NFIX as a crucial regulator of NSC differentiation [15]. Harris and colleagues [15] showed that $Nfix$ deletion leads to prolonged self-renewal of NSCs in the embryonic mouse forebrain, resulting in the overproduction of neurons and astrocytes. Furthermore, transcriptomic sequencing analyses of the human fetal brain have shown enrichment of the NFI family of transcription factors as key regulatory elements during neurodevelopment [45]. In line with this, our data indicate that an increased period of progenitor cell self-renewal, and hence ultimately more post-mitotic progeny, could underlie the macrocephalic phenotype of Malan syndrome patients. Notably, while our data shows that $Nfix$ heterozygous animals have an increased corpus callosum volume, this is in contrast to the typical corpus callosum hypoplasia occasionally exhibited by Malan syndrome patients. We propose that future clinical assessment of Malan syndrome patients should further examine brain size to validate whether Malan patients have megalencephaly in addition to macrocephaly.

Currently, detailed neuroanatomical and behavioral studies are also lacking in Malan syndrome patients [5]. Here, we demonstrate that disruption in the structural connectivity of the brain manifest as deficits in cortically-controlled behavior. These findings provide key insights into
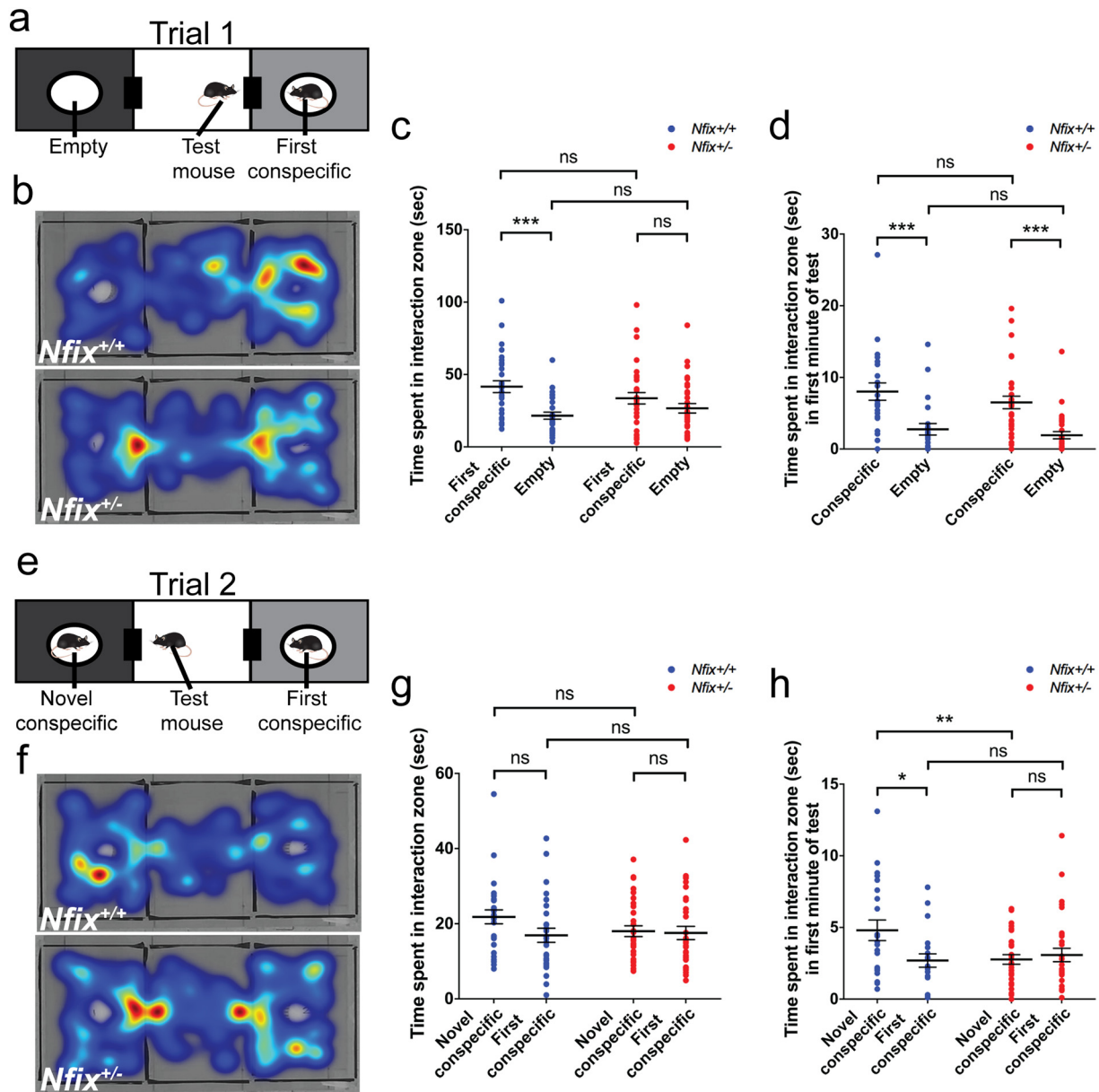
Fig. 6. *Nfix*^{+/−} mice display abnormal social behavior. Adult *Nfix*^{+/+} control (*n* = 29) and *Nfix*^{+/−} mice (*n* = 32) performed the 3-chambered sociability task for 5 min in two trials. (**a**) Trial 1 examined social approach behavior and (**e**) trial 2 tested preference for social novelty. (**b, e**) Representative images of Ethovision™XT tracking shown in trial 1 and 2. (**b, c**) In the total 5-min period of trial 1, control animals spent significantly more time with the conspecific mouse compared to the empty cage, thus, indicating social approach. *Nfix*^{+/−} mice demonstrated no difference in the time spent with the conspecific mouse compared to the empty cage. (**d**) Within the first minute of trial 1, control and *Nfix*^{+/−} animals spent significantly longer with the conspecific mice compared to the empty cage. (**e, g**) During the total period of trial 2, control and *Nfix*^{+/−} adult mice showed no differences in the time spent interacting with the novel conspecific mouse compared the first conspecific mice. (**f, h**) However, during the first minute of introducing the novel conspecific in trial 2, *Nfix*^{+/+} mice displayed significant preferential interaction with the novel conspecific mice over the first conspecific mice, comparatively *Nfix*^{+/−} mice showed no preference for social novelty. Data are represented as mean ± SEM. (ns) not significant, *p < .05; **p < .01; ***p < .001, two-way ANOVA.

the intellectual disability and autistic-like traits featured in Malan syndrome patients. Notably, structures within the limbic and frontal cortex circuitry were significantly affected in the *Nfix*^{+/−} mouse brain (Fig. 4). These animals further exhibited learning and memory impairments (Fig. 5), and abnormal social behavior (Fig. 6). The interconnected structures of the limbic system are critical in memory consolidation, emotional processing, such as anxiety, fear and aggression, and stress-response [46,47], while the prefrontal cortex is responsible for executive functions and moderating social behaviors [41,46]. Interestingly, Malan syndrome patients have been reported to exhibit moderate to severe intellectual disability, autistic spectrum disorder traits, high anxiety levels, sensitivity to noise, and aggressive behavior [1,3,5]. The association between changes in brain connectivity and abnormal behavior have previously been reported in other developmental disorders,

such as autism spectrum disorder. Neuroimaging studies of autistic patients reported increased connectivity in the basal ganglia and paralimbic-limbic system [48], and decreased connectivity in the supplementary motor area and sub regions of the prefrontal cortex [48,49]. Aberrant axonal integrity of the anterior commissure and corpus callosum was also found in autistic patients [50] and in mouse models of autism spectrum disorder [51]. This correlates with our tractography data, which shows that *Nfix* heterozygous brains have a loss of axonal integrity in the corpus callosum, anterior commissure, and hippocampal commissure (Fig. 2 and Fig. 3). Deficits in learning and memory function in *Nfix*^{+/−} mice is likely underlined by reduced hippocampal neurogenesis [17], which is known to be critical for learning and memory function [52,53]. Collectively, it is likely that intellectual disability and autistic-like traits exhibited by Malan syndrome

patients is underlined by deficits in hippocampal neurogenesis and aberrant structural connectivity within the limbic-prefrontal circuitry. However, as detailed cognitive and behavioral studies are still lacking in Malan syndrome patients, future cognitive assessment of Malan syndrome patients could involve structural MRI and connectome analyses to provide insight into the cortical abnormalities underlying the intellectual disability in these patients.

Further studies are required to understand the abnormal developmental processes leading to Malan syndrome. For example, *in vitro* assays could be used to assess whether *Nfix* deficiency disrupts neurite growth and axonal guidance, processes that may underlie the aberrant axonal integrity of commissural tracts found in adult *Nfix*$^{+/-}$ brains. The generation, and subsequent migration, of cortical neuronal populations could also be examined using BrdU/EdU pulse-chase labelling. Further characterization of the cellular populations within the *Nfix* heterozygous neocortex may also include additional layer specific markers, such as Tbr1, Brn1 and Cux1, as well as an analysis of the ratio of excitatory and inhibitory neurons. NFIX is also expressed by many mature neurons within the rodent neocortex [16], but the role of NFIX in these cells is completely undefined. Electrophysiological experiments would further provide insights into how overgrowth and abnormal connectivity within *Nfix* heterozygous brains may affect changes in circuit-level plasticity and function. Moreover, while social interaction behavior is a key diagnostic measure of autism spectrum disorder, other key features include repetitive stereotypic behaviors and communication deficits [40]. To assess repetitive behaviors, further assays can include the automated 16-hole nose poke task to assess restricted interest [40], and/or examine home-cage stereotypes [54]. Communication within rodents can be assessed using ultrasonic vocalization tests and/or olfactory habituation/dishabituation to urinary pheromones tests [40].

In conclusion, by modelling brain structure and behavior in *Nfix* heterozygous mice, we provide a significant conceptual advance in our understanding of the factors underlying Malan syndrome. These findings suggest that future assessments of Malan syndrome patients could examine the presence of megalencephaly and high-resolution neuroimaging, such as DTMRI and tractography.

Acknowledgements

Funding

Author contributions

Conceived and designed the experiments: S.O., D.H., N.D.K., and M.P. Performed the experiments: S.O., D.H., N.D.K., and M.K. Analyzed the data: S.O., D.H., N.D.K., L.H., O.Z., T.H.J.B., and M.P. Contributed reagents/materials/analysis tools: N.D.K., L.H., O.Z., T.H.J.B., and R.M.G. Writing – original draft: S.O. and M.P. All authors read and approved the final manuscript.

Declaration of interests

Dr. Gronostajski reports grants from NYSTEM, other from New York State Government, during the conduct of the study (outside of the work). All other authors declare no competing or financial interests.

Appendix A. Supplementary data

Supplementary data to this article can be found online at https://doi.org/10.1016/j.ebiom.2018.11.044.

References

[1] Malan V, Rajan D, Thomas S, Shaw AC, Louis Dit Picard H, Layet V, et al. Distinct effects of allelic NFIX mutations on nonsense-mediated mRNA decay engender either a Sotos-like or a Marshall-Smith syndrome. Am J Hum Genet 2010;87(2):189–98.

[2] Gurrieri F, Cavaliere ML, Wischmeijer A, Mammi C, Neri G, Pisanti MA, et al. NFIX mutations affecting the DNA-binding domain cause a peculiar overgrowth syndrome (Malan syndrome): a new patients series. Eur J Med Genet 2015;58(9):488–91.

[3] Klaassens M, Morrogh D, Rosser EM, Jaffer F, Vreeburg M, Bok LA, et al. Malan syndrome: Sotos-like overgrowth with de novo NFIX sequence variants and deletions in six new patients and a review of the literature. Eur J Hum Genet 2015;23(5):610–5.

[4] Yoneda Y, Saitsu H, Touyama M, Makita Y, Miyamoto A, Hamada K, et al. Missense mutations in the DNA-binding/dimerization domain of NFIX cause Sotos-like features. J Hum Genet 2012;57(3):207–11.

[5] Priolo M, Schanze D, Tatton-Brown K, Mulder PA, Tenorio J, Kooblall K, et al. Further delineation of Malan syndrome. Hum Mutat 2018;39(9):1226–37.

[6] Demyer W. Megalencephaly: types, clinical syndromes, and management. Pediatr Neurol 1986;2(6):321–8.

[7] Pavone P, Praticò AD, Rizzo R, Corsello G, Ruggieri M, Parano E, et al. A clinical review on megalencephaly. Medicine 2017;96(26):e6814.

[8] Winden KD, Yuskaitis CJ, Poduri A. Megalencephaly and macrocephaly. Semin Neurol 2015;35(3):277–87.

[9] Campbell CE, Piper M, Plachez C, Yeh YT, Baizer JS, Osinski JM, et al. The transcription factor Nfix is essential for normal brain development. BMC Dev Biol 2008;8:52.

[10] Harris L, Dixon C, Cato K, Heng YH, Kurniawan ND, Ullmann JF, et al. Heterozygosity for nuclear factor one x affects hippocampal-dependent behaviour in mice. PLoS One 2013;8(6):e65478.

[11] Heng YH, McLeay RC, Harvey TJ, Smith AG, Barry G, Cato K, et al. NFIX regulates neural progenitor cell differentiation during hippocampal morphogenesis. Cereb Cortex 2014;24(1):261–79.

[12] Piper M, Harris L, Barry G, Heng YHE, Plachez C, Gronostajski RM, et al. Nuclear factor one X regulates the development of multiple cellular populations in the postnatal cerebellum. J Comp Neurol 2011;519(17):3532–48.

[13] Driller K, Pagenstecher A, Uhl M, Omran H, Berlis A, Grunder A, et al. Nuclear factor I X deficiency causes brain malformation and severe skeletal defects. Mol Cell Biol 2007;27(10):3855–67.

[14] Messina G, Biressi S, Monteverde S, Magli A, Cassano M, Perani L, et al. Nfix regulates fetal-specific transcription in developing skeletal muscle. Cell 2010;140(4):554–66.

[15] Harris L, Zalucki O, Gobius I, McDonald H, Osinki J, Harvey TJ, et al. Transcriptional regulation of intermediate progenitor cell generation during hippocampal development. Development 2016;143(24):4620–30.

[16] Chen KS, Harris L, Lim JWC, Harvey TJ, Piper M, Gronostajski RM, et al. Differential neuronal and glial expression of nuclear factor I proteins in the cerebral cortex of adult mice. J Comp Neurol 2017;525(11):2465–83.

[17] Harris L, Zalucki O, Clément O, Fraser J, Matuzelski E, Oishi S, et al. Neurogenic differentiation by hippocampal neural stem and progenitor cells is biased by NFIX expression. Development 2018;145(3):dev155689.

[18] Zalucki O, Harris L, Harvey TJ, Harkins D, Widagdo J, Oishi S, et al. NFIX-mediated inhibition of neuroblast branching regulates migration within the adult mouse ventricular-subventricular zone. Cereb Cortex 2018. https://doi.org/10.1093/cercor/bhy233 [Epub ahead of print].

[19] Kurniawan ND. MRI in the study of animal models of neurodegenerative diseases. In: García Martín ML, López Larrubia P, editors. Preclinical MRI: Methods and Protocols. New York, NY: Springer New York; 2018. p. 347–75.

[20] Tournier J, Calamante F, Connelly A. MRtrix: Diffusion tractography in crossing fiber regions. Int J Imaging Syst Technol 2012;22(1):53–66.

[21] Ma Y, Hof PR, Grant SC, Blackband SJ, Bennett R, Slatest L, et al. A three-dimensional digital atlas database of the adult C57BL/6J mouse brain by magnetic resonance microscopy. Neuroscience 2005;135(4):1203–15.

[22] Calamante F, Tournier JD, Kurniawan ND, Yang Z, Gyengesi E, Galloway GJ, et al. Super-resolution track-density imaging studies of mouse brain: comparison to histology. Neuroimage 2012;59(1):286–96.

[23] Alexander AL, Hurley SA, Samsonov AA, Adluru N, Hosseinbor AP, Mossahebi P, et al. Characterization of cerebral white matter properties using quantitative magnetic resonance imaging stains. Brain Connect 2011;1(6):423–46.

[24] Liu C, Li Y, Edwards TJ, Kurniawan ND, Richards LJ, Jiang T. Altered structural connectome in adolescent socially isolated mice. Neuroimage 2016;139:259–70.

[25] Zalesky A, Fornito A, Bullmore ET. Network-based statistic: identifying differences in brain networks. Neuroimage 2010;53(4):1197–207.

[26] Oishi S, Premarathne S, Harvey TJ, Iyer S, Dixon C, Alexander S, et al. Usp9x-deficiency disrupts the morphological development of the postnatal hippocampal dentate gyrus. Sci Rep 2016;6:25783.

[27] Peca J, Feliciano C, Ting JT, Wang W, Wells MF, Venkatraman TN, et al. Shank3 mutant mice display autistic-like behaviours and striatal dysfunction. Nature 2011;472 (7344):437–42.

[28] Stuchlík A, Petrásek T, Prokopová I, Holubová K, Hatalová H, Valeš K, et al. Place avoidance tasks as tools in the behavioral neuroscience of learning and memory. Physiol Res 2013;62(Suppl. 1):S1–S19.

[29] Zalucki O, Harkins D, Harris L, Burne THJ, Gronostajski RM, Piper M. Analysis of hippocampal-dependent learning and memory behaviour in mice lacking Nfix from adult neural stem cells. BMC Res Notes 2018;11(1).

[30] Chaudhry AZ, Lyons GE, Gronostajski RM. Expression patterns of the four nuclear factor I genes during mouse embryogenesis indicate a potential role in development. Dev Dyn 1997;208(3):313–25.

[31] Dimou L, Gotz M. Glial cells as progenitors and stem cells: new roles in the healthy and diseased brain. Physiol Rev 2014;94(3):709–37.

[32] Britanova O, de Juan Romero C, Cheung A, Kwan KY, Schwark M, Gyorgy A, et al. Satb2 is a postmitotic determinant for upper-layer neuron specification in the neocortex. Neuron 2008;57(3):378–92.

[33] Chen B, Wang SS, Hattox AM, Rayburn H, Nelson SB, McConnell SK. The Fezf2-Ctip2 genetic pathway regulates the fate choice of subcortical projection neurons in the developing cerebral cortex. Proc Natl Acad Sci U S A 2008;105(32):11382–7.

[34] Raponi E, Agenes F, Delphin C, Assard N, Baudier J, Legraverend C, et al. S100B expression defines a state in which GFAP-expressing cells lose their neural stem cell potential and acquire a more mature developmental stage. Glia 2007;55(2):165–77.

[35] Mei F, Wang H, Liu S, Niu J, Wang L, He Y, et al. Stage-specific deletion of Olig2 conveys opposing functions on differentiation and maturation of oligodendrocytes. J Neurosci 2013;33(19):8454–62.

[36] Rivers LE, Young KM, Rizzi M, Jamen F, Psachoulia K, Wade A, et al. PDGFRA/NG2 glia generate myelinating oligodendrocytes and piriform projection neurons in adult mice. Nat Neurosci 2008;11(12):1392–401.

[37] Cimadevilla JM, Kaminsky Y, Fenton A, Bures J. Passive and active place avoidance as a tool of spatial memory research in rats. J Neurosci Methods 2000;102(2):155–64.

[38] Dockery CA, Wesierska MJ. A spatial paradigm, the allothetic place avoidance alternation task, for testing visuospatial working memory and skill learning in rats. J Neurosci Methods 2010;191(2):215–21.

[39] Dawson G, Webb S, Schellenberg GD, Dager S, Friedman S, Aylward E, et al. Defining the broader phenotype of autism: genetic, brain, and behavioral perspectives. Dev Psychopathol 2002;14(3):581–611.

[40] Moy SS, Nadler JJ, Poe MD, Nonneman RJ, Young NB, Koller BH, et al. Development of a mouse test for repetitive, restricted behaviors: relevance to autism. Behav Brain Res 2008;188(1):178–94.

[41] Forbes CE, Grafman J. The role of the human prefrontal cortex in social cognition and moral judgment. Annu Rev Neurosci 2010;33:299–324.

[42] Fenlon LR, Liu S, Gobius I, Kurniawan ND, Murphy S, Moldrich RX, et al. Formation of functional areas in the cerebral cortex is disrupted in a mouse model of autism spectrum disorder. Neural Dev 2015;10:10.

[43] Kaidanovich-Beilin O, Lipina T, Vukobradovic I, Roder J, Woodgett JR. Assessment of social interaction behaviors. J Vis Exp 2011(48).

[44] Vidovic D, Harris L, Harvey TJ, Evelyn Heng YH, Smith AG, Osinski J, et al. Expansion of the lateral ventricles and ependymal deficits underlie the hydrocephalus evident in mice lacking the transcription factor NFIX. Brain Res 2015;1616:71–87.

[45] Luo C, Lancaster MA, Castanon R, Nery JR, Knoblich JA, Ecker JR. Cerebral organoids recapitulate epigenomic signatures of the human fetal brain. Cell Rep 2016;17 (12):3369–84.

[46] Ko J. Neuroanatomical substrates of rodent social behavior: the medial prefrontal cortex and its projection patterns. Front Neural Circuits 2017;11:41.

[47] Martin EI, Ressler KJ, Binder E, Nemeroff CB. The neurobiology of anxiety disorders: brain imaging, genetics, and psychoneuroendocrinology. Psychiatric Clinics of North America 2009;32(3):549–75.

[48] Li SJ, Wang Y, Qian L, Liu G, Liu SF, Zou LP, et al. Alterations of white matter connectivity in preschool children with autism spectrum disorder. Radiology 2018;288(1): 209–17.

[49] Rane P, Cochran D, Hodge SM, Haselgrove C, Kennedy DN, Frazier JA. Connectivity in autism: a review of mri connectivity studies. Harv Rev Psychiatry 2015;23(4): 223–44.

[50] Chiang HL, Chen YJ, Lin HY, Tseng WI, Gau SS. Disorder-specific alteration in white matter structural property in adults with autism spectrum disorder relative to adults with adhd and adult controls. Hum Brain Mapp 2017;38(1):384–95.

[51] Ellegood J, Babineau BA, Henkelman RM, Lerch JP, Crawley JN. Neuroanatomical analysis of the BTBR mouse model of autism using magnetic resonance imaging and diffusion tensor imaging. Neuroimage 2013;70:288–300.

[52] Goncalves JT, Schafer ST, Gage FH. Adult neurogenesis in the hippocampus: from stem cells to behavior. Cell 2016;167(4):897–914.

[53] Spalding KL, Bergmann O, Alkass K, Bernard S, Salehpour M, Huttner HB, et al. Dynamics of hippocampal neurogenesis in adult humans. Cell 2013;153(6):1219–27.

[54] Silverman JL, Yang M, Lord C, Crawley JN. Behavioural phenotyping assays for mouse models of autism. Nat Rev Neurosci 2010;11(7):490–502.